# Traveling-Wave Tube Amplifier Performance Evaluation and Design Optimization for Applications in Digital Communications With Multilevel Modulations

Joe X. Qiu, *Member, IEEE*, David K. Abe, *Member, IEEE*, Thomas M. Antonsen, Jr., *Senior Member, IEEE*, Bruce G. Danly, *Fellow, IEEE*, and Baruch Levush, *Fellow, IEEE*

***Abstract*—In this paper, we demonstrate the use of a power margin as a figure-of-merit for evaluating the performance and optimizing the design of traveling-wave tube amplifiers (TWTAs) used in digital communication applications with multilevel modulations. The power margin is a system-level measure that balances both device efficiency and nonlinear distortion and provides a more direct prediction of the system-level performance of power amplifiers than device-level measures such as device efficiency or error-vector-magnitude. We calculate the power margin for M quadrature amplitude modulation for an existing TWTA to demonstrate the setting of an optimal amplifier operating drive level according to the criterion of the maximum power margin. The power margin can also be used to compare the performance of different traveling-wave tube (TWT) configurations. We compare the calculated power-margin performance for helix TWT circuits optimized with different optimization goal functions using the helix TWT design code CHRISTINE. The goal functions used in the optimization of the TWT circuits include AM/PM optimization, complex gain optimization, efficiency optimization, and a new digital goal function optimization. The digital goal function is shown to provide an enhanced power margin compared to the other three goal functions and demonstrates the potential of TWT device design optimization from a system perspective.**

***Index Terms*—Communication systems, microwave circuit optimization, microwave power amplifiers (PAs), nonlinear distortion, satellite communication, traveling-wave tubes (TWTs).**

## I. Introduction

THE increasing need for high data rate (HDR) links in military and commercial communication systems, coupled with the limitation on available spectrum, is resulting in a renewed interest in high spectral-efficiency modulations. For the designer of power amplifiers (PAs) to be utilized in these new systems, the use of multilevel modulations places a stringent requirement on PA linearity. Whether one is concerned with the battery life of a cell phone with a solid-state monolithic microwave integrated circuit (MMIC) amplifier or the power budget in a satellite communications system employing a traveling-wave tube amplifier (TWTA), the system objective is the same, namely, maximizing link margin while minimizing prime power requirements. From the device perspective, this translates to the objective of minimizing distortion while maximizing device efficiency. The design of PAs to optimally achieve this objective is the subject of much research.

This paper demonstrates a procedure for the optimal design of a TWTA using the power margin in a communication link as the figure-of-merit. The power margin is the ratio of the available power to the power needed to maintain a specified bit error rate (BER) in the presence of a known level of additive noise. While the power margin for a particular design depends on a number of specific parameters such as noise level and error rate, the ratio of power margins for two designs does not. Thus, the power margin is a measure of the performance of an amplifier design.

It is shown that the optimization procedure based on the power margin can be used not only for setting the operating point of the TWTA, but also for optimization of the physical design of the traveling-wave tube (TWT) itself. The use of TWTAs designed by such a procedure can, in principle, yield an improvement in the system link margin over systems employing TWTAs designed according to more traditional analog distortion specifications. Furthermore, it has become increasingly common for a system to use a TWTA in combination with a predistortion linearizer to reduce the nonlinear distortion by the TWTA [1]. It is possible to extend the design technique to optimize a TWT circuit to achieve a particular set of AM/AM and AM/PM drive curves that can better match the characteristic of a linearizer in order to achieve maximum compensation. Similarly, the need for higher data rate places increasing bandwidth requirements on PAs and demands unprecedented wide-band nonlinear modeling of PAs [2]. The technique described here can also be extended to include power margin degradation due to memory effects and to optimize power-margin performance of TWT circuits with wide-band nonlinear memory effects taken in account.

In this paper, we will concentrate on applications where the bandwidth of the digitally modulated signal being amplified by the TWTA is relatively narrow so that the gain is independent of frequency and the memoryless nonlinear model [3], [4] for the

Manuscript received August 21, 2002; revised January 23, 2003. This work was supported by the Office of Naval Research.

J. X. Qiu, D. K. Abe, B. G. Danly, and B. Levush are with the Vacuum Electronics Branch, Naval Research Laboratory, Washington, DC 20375 USA (e-mail: qiu@estd.nrl.navy.mil).

T. M. Antonsen, Jr. is with the Department of Electrical Engineering and Department of Physics, University of Maryland at College Park, College Park, MD 20742 USA and also with the Science Applications International Corporation, McLean, VA 22101 USA.

Digital Object Identifier 10.1109/TMTT.2003.815266

TWT can be applied. In these types of applications, two issues are of great importance.

The first is, for an existing TWTA, the determination of optimal drive level. The conflicting requirements of efficiency and linearity prevent the TWTA from operating near saturation; on the other hand, operating the TWTA with low efficiency would be economically undesirable. From the system perspective, optimal operation of a TWTA requires the tradeoff between power and distortion. Significant efforts have been devoted to the study of this issue. Criteria based on analog figures-of-merit such as noise power ratio (NPR) have been suggested for this purpose [5]. The shortcoming of analog figures-of-merit is their failure in revealing the digital nature of the communication signals. Alternatively, power-margin analysis based on system-level digital error rates is often used to optimize the PA operating point [6]. The inverse of a power margin is also referred to as total degradation in the literature [7].

The second issue is the optimization of the TWT design to achieve the highest possible performance. Dynamic velocity tapering (DVT) is a well-known technique to improve the efficiency and linearity of TWTs by properly varying circuit physical parameters such as helix-pitch profiles [8], [9], and a great number of similar techniques have also been invented to improve the efficiency and linearity of TWTs over the past 50 years [10]–[13]. With the recent advances in high-fidelity computer modeling of TWTs and the rapid increase in computing speed, it is possible to quickly evaluate TWT circuits and perform iterative optimizations by changing circuit parameters using feedback from the circuit evaluation. The physics-based helix TWT design code CHRISTINE is one example of a modern high-fidelity TWT design code [14], [15]. The question of which goal function to use in the optimizer must then be answered. Traditional performance specification of a TWT such as AM/AM and AM/PM distortion provides only limited insight in addressing the issue. Direct optimization of TWT circuits using system-level figures-of-merit such as a power margin should prove to be advantageous.

This paper is organized as follows. In Section II, a memoryless nonlinear model of the TWT is described. In Section III, we calculate the power-margin performance of a TWTA using square M quadrature amplitude modulation (M-QAM). This modulation has been chosen as representative of a multilevel modulation, which would require significantly better linearity in the PA than more traditional near constant-envelope modulations [minimum phase-shift keying (MSK), binary phase-shift keying (BPSK), quadrature phase-shift keying (QPSK)]. In Section IV, we make use of CHRISTINE's optimization capabilities to illustrate the design of helix TWT circuits, which are optimized for link power margin. The power margin for the optimized TWT circuits is calculated to compare the relative performance of the circuits. The goal functions used include AM/PM minimization, complex gain linearization, efficiency maximization, and a new digital goal function that is an approximation of the exact power-margin calculation.

## II. Memoryless Nonlinear Model for TWTA

If the bandwidth used in a modulated carrier communication system is small enough such that the amplifier transfer characteristic is essentially frequency independent over the bandwidth of the signal, the amplifier is traditionally modeled by the instantaneous nonlinear amplitude and phase transfer functions.

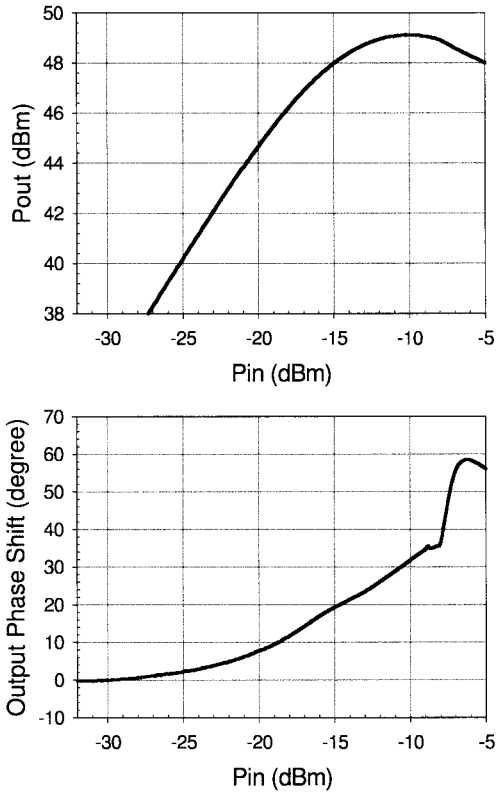


Fig. 1. Measured nonlinear gain and phase conversion functions for the Hughes 8573H helix TWTA at 1.65 GHz.

Assume the complex envelope of the RF input signal is given by

$$x(t) = A(t)\exp\left[i \cdot \phi(t)\right] \tag{1}$$

where $A(t)$ and $\phi(t)$ are the instantaneous amplitude and phase of the RF waveform. The digital information is carried by $A(t)$ and $\phi(t)$, whose exact forms depend on the modulation formats. The output through a memoryless nonlinearity can be written as

$$y(t) = f\left[A(t)\right]\exp\left\{i \cdot g\left[A(t)\right] + i \cdot \phi(t)\right\} \tag{2}$$

where $f(A)$ and $g(A)$ are the nonlinear amplitude and phase transfer curves obtained from single-tone swept-power measurement. The experimental nonlinear transfer curves for a Hughes 8573H helix TWTA at 1.65 GHz are shown in Fig. 1, where the magnitudes of the input and output signals are expressed as powers measured in dBm.

## III. Performance Evaluation of TWTA Using a Power Margin

### A. Definition of a Power Margin

The probability of demodulation error at the receiver is typically the prime performance measure in digital communication systems. A demodulation error occurs when the demodulated location of a signal falls outside of the decision boundary of its associated reference constellation. When the received signal

is corrupted by additive white Gaussian noise (AWGN), the symbol error rate (SER) can be estimated by integrating the portion of a two-dimensional (2-D) Gaussian distribution outside the decision boundary of a particular reference. Assuming a square M-QAM constellation is gray-coded, the BER is given by

$$\mathrm{BER} = \frac{\mathrm{SER}}{\log_2 M} \tag{3}$$

where $M$ is the modulation order.

For a perfect linear amplifier, increasing the input drive will increase the output power and the carrier-to-noise ratio (CNR) and, therefore, lower the BER. In the presence of nonlinear distortion, a higher CNR is needed with increasing input drive in order to achieve the same BER. Such an increase in CNR and the accompanying increase in the required power represent a power penalty for operating an amplifier in its nonlinear regime.

A quantitative measure by which amplifiers can be designed and operating points can be chosen is to compute the power margin. The power margin is defined as the ratio between the available power and the power needed to sustain a particular BER level with a known noise level [6]. The absolute value of the power margin depends on a number of other system specific factors in a communication link: antennas, path losses, and noise levels, etc., which are not the concern of this paper. The important features of the power-margin curve remain unchanged as long as the nonlinearity is fixed. Therefore, the power-margin curve can be very useful for setting the optimal operating point for an existing TWTA, as well as comparing the relative performance of different TWT designs.

In Fig. 2, we plot the calculated power margin for the Hughes 8573H TWTA at 1.65 GHz for M-QAM modulation for $M = 16, 32, 64$, and 128 and a reference BER of $10^{-5}$. The power margin is normalized to the maximum achievable power margin for $\mathrm{M} = 16$ for a linear amplifier with the power for the largest amplitude symbol equal to the saturation power of the TWTA. The curve indicates that the TWTA's optimal operation requires significant backoff from saturation and the amount of the backoff depends on the modulation format used for the system. The higher the modulation order, the greater the backoff and the lower the achievable power margin. The constellations and decision boundaries used in the calculation are generated by requiring that

$$\frac{1}{M}\sqrt{\sum_{i=1}^{M} |y_i - \lambda x_i|^2} \tag{4}$$

is minimized, where $M$ is the modulation order, $y_i$ is the recovered transmitted symbols, $x_i$ is the ideal constellation reference and $\lambda$ is a complex scaling factor. The amplitude of $\lambda$ is related to signal gain estimation and its phase is related to carrier phase estimation. The exact values of $x_i$ depend on the modulation. For 16 QAM, in a complex baseband notation, $x_i \in \{x | \pm 1 \pm i, \pm 1 \pm 3i, \pm 3 \pm i, \pm 3 \pm 3i\}$ and $y_i$ is related to $x_i$ according to (2).

Finally we note that, in our calculation of the BER, coding and its effect on the BER are not considered. In a nonlinear channel, the use of coded M-QAM signals can have the benefits of lowering the BER and providing a power-margin gain [16].

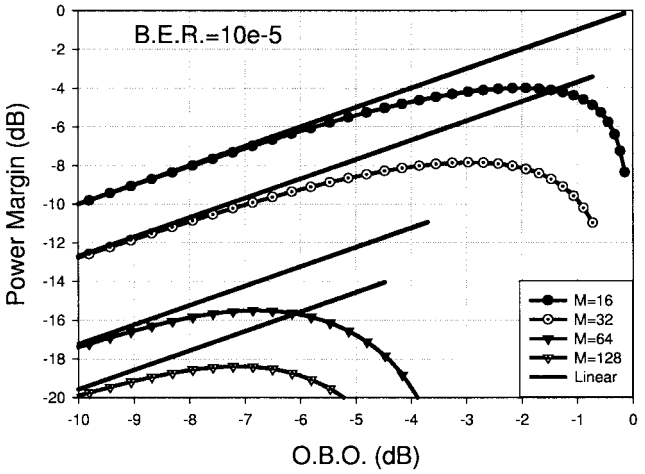


Fig. 2. Power margin for M-QAM versus peak output backoff (O.B.O.) from saturation.

### *B. Power Margin Versus Spectral Regrowth*

Spectral regrowth and spectral-regrowth-derived parameters such as adjacent channel power ratio (ACPR) have long been used as figures-of-merit for measuring the nonlinear distortion in a microwave PA. Spectral regrowth, however, does not reveal any information on device efficiency. Furthermore, it also shows little dependence on the signal modulation. On the other hand, the values of the power margin show strong dependence on both the input drive and modulation order.

We note that, despite the relative insensitivity of spectral regrowth on modulation information, they remain important requirements for multichannel applications and government spectrum regulation.

## IV. TWT Circuit Design Optimization Using a Power Margin

The power margin also provides a means for comparing the performance of TWT circuit designs from a system perspective and can be used as a figure-of-merit for optimizing TWT circuit design. The TWT design code CHRISTINE has the capability of optimizing circuit parameters using a modified steepest descent algorithm to achieve desired performance characteristics depending on the specified goal functions. The circuit parameters that can be varied are those describing the circuit (pitch profile, helix radius, vane radius, etc.). Here, we use the power margin for 16-QAM modulation as a figure-of-merit to compare the performance for different circuit designs for a $C$-band helix TWT at 5 GHz optimized with four different goal functions. The goal functions that we have experimented with are as follows.

1) AM/PM optimization

$$\mathrm{Error}_{\mathrm{phase}} = \int_0^{P_{\max}} \frac{dP_{\mathrm{out}}}{P_{\max}} \left|\phi(P_{\mathrm{in}}) - \phi(0)\right| \tag{5}$$

is minimized, where $\phi(P_{\mathrm{in}})$ is the output phase shift and $P_{\max}$ is a specified maximum output power.

2) Complex gain optimization

$$\text{Error}_{\text{gain}} = \int_0^{P_{\max}} \frac{dP_{\text{out}}}{P_{\max}} \left| \frac{G(P_{\text{in}}) - G(0)}{G(0)} \right| \tag{6}$$

is minimized, where $G(P_{\text{in}})$ is the complex gain and $P_{\max}$ is a specified maximum output power.

3) Efficiency optimization

$$\eta = \frac{P_{\text{out}} - P_{\text{in}}}{IV} \tag{7}$$

is maximized, where $I$ and $V$ are the beam current and voltage, respectively.

4) Digital optimization:

$$\text{Power\_margin}_{\text{digital}} = \overline{P}_{\text{out}}(\text{dB}) - 10\frac{1}{n}\log_{10}\left(\sum_{i=1}^{m}\left(\frac{D}{d_i^s}\right)^{2n}\right) \tag{8}$$

is maximized, where $\overline{P}_{\text{out}}$ is the average power of the recovered symbols at the moment of symbol decision, $D$ is the distance from an element of the ideal reference constellation to its decision boundary, $d_1^s$ is the shortest distance for all the recovered symbols to their decision boundaries in the first quadrant of the in-phase/quadrature (I/Q) plane, $d_2^s$ is the second shortest distance, and so on, as shown in Fig. 3. The choices of parameters $m$ and $n$ depend on the order of the M-QAM modulation and are listed in the Appendix. For 16 QAM, $m = 4$ and $n = 6.5$.

Goal functions 1–3 have traditionally been used in optimizing TWT designs for analog applications [17]. Their definitions do not contain system-level information so it is unlikely for them to result in designs that produce an optimal power margin. The definition of a power margin requires simultaneous optimization of efficiency and linearity.

Goal function 4, as derived in the Appendix , is an approximation of the power margin and should produce that highest power margin. It is motivated by the principle of union bound, which is based on the distances from the transmitted symbols to their associated decision boundaries [18], [19]. The reason for using an approximation in implementing the power margin as a goal function instead of the exact power-margin calculation is to reduce computation time. With the present implementation of the digital goal function in CHRISTINE, most of the computation time during optimization is consumed by calculations of physical processes in the TWT. (Total computation time for each digital optimization run is approximately 3 h on a 1.33-GHz Athlon personal computer (PC).) With the availability of faster CPUs, this computation time will surely be decreased and the approximation for the power margin may be replaced by the exact calculation without run-time penalty.

Both the complex gain and AM/PM optimization require the choices of a $P_{\max}$ in output power and a corresponding $P_{\text{in\_max}}$ in input power for the goal function so that a minimum linear gain $P_{\max}/P_{\text{in\_max}}$ must be maintained for a successful optimization run [17].

The electron-beam parameters and helix-circuit parameters other than the helix-pitch profile for the $C$-band helix TWT used in the optimization were the same as those listed in [17]. To arrive at each of the optimized designs for the $C$-band helix TWT using a particular goal function, helix-pitch profiles after the sever were varied beginning with a constant profile as the initial condition, while all other circuit parameters were held fixed to achieve the desired optimization. The electron beam current and voltage (and, therefore, beam power) were also fixed so that efficiencies could be compared. Second harmonic production was also included in the simulation.

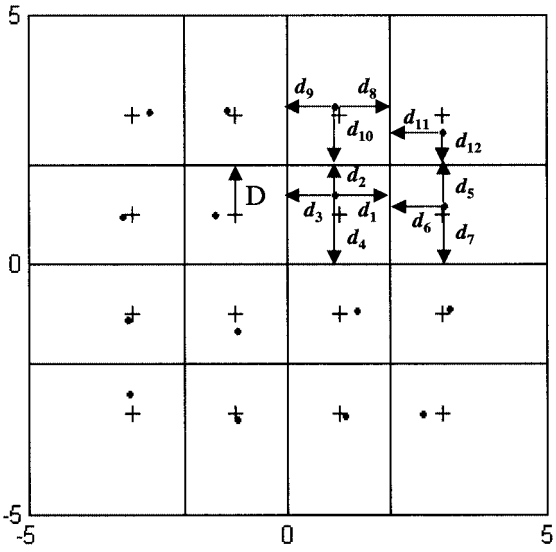


Fig. 3. Geometrical distribution of the reference constellations (+) and recovered symbols (.) for 16-QAM. Distance from the reference constellations to the decision boundaries is $D$. Distances from the recovered symbols to the decision boundaries are $d_i$. $d_1^s$ is the shortest distance, $d_2^s$ is the second shortest distance, and so on.

Two approaches for varying the helix-pitch profile were used. In the first approach, the helix pitch at 11 fixed locations along the helix after the sever was allowed to vary freely and the pitch between those fixed points was obtained by linear interpolation from the two nearest fixed points. In the second approach, the helix-pitch profile was forced to vary according to some predefined curves with parameters relating to the shape of those curves as the optimization parameters.

### A. Freely Varying Helix-Profile Optimization

Four optimized helix circuits were obtained for the four goal functions using this approach. The characteristics for each of the circuits are shown in Figs. 4–7. The drive curves are shown in Figs. 4 and 5, the helix-pitch profile is shown in 6 and the power margin is shown in 7. The power-margin curves are calculated by estimating the BER using the drive curves in Figs. 4 and 5 with a reference BER of $10^{-5}$ for 16 QAM. The fact that a circuit optimized with the digital goal function has the highest power margin and achieves a 1-dB improvement in the power margin compared to the constant pitch case demonstrates that it is possible to optimize a TWT circuit according to system-level information such as modulation format, communication standards, and power margin, etc.

Of the four goal functions, AM/PM optimization yields an even lower power margin than the untapered unoptimized circuit because of the lower available output power. It is obvious

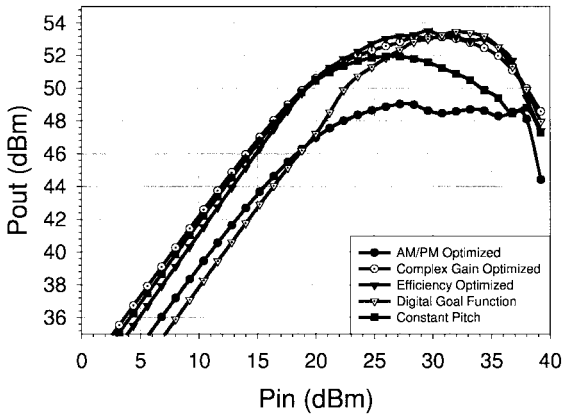


Fig. 4. Nonlinear amplitude conversion for the optimized helix TWT circuits.

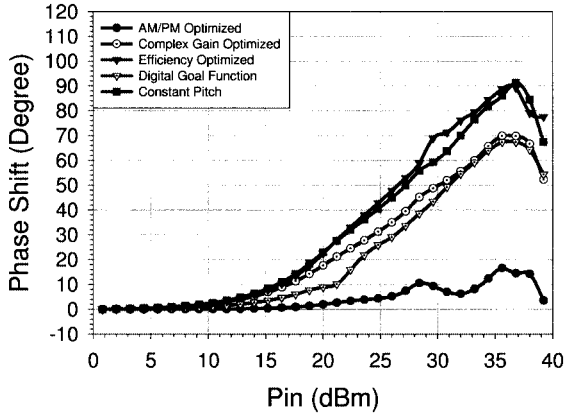


Fig. 5. Nonlinear phase conversion for the optimized helix TWT circuits.

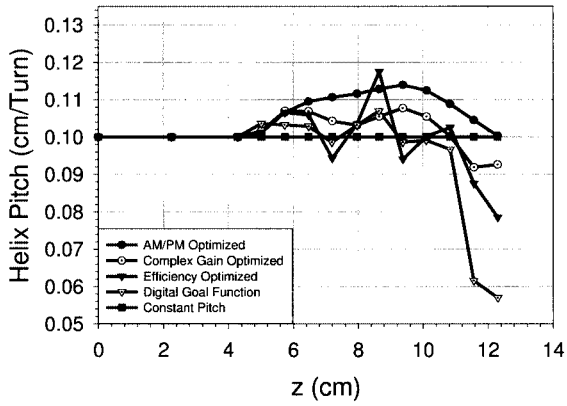


Fig. 6. Helix profiles for the optimized helix TWT circuits.

that this is not an acceptable optimization strategy. Efficiency optimization and complex gain optimization are two commonly used goal functions for optimizing TWT circuits. The shortcoming of efficiency optimization is its inattention to nonlinear distortion.

It may be possible to improve the power margin further for complex gain optimization by changing $P_{\max}$ and $P_{\text{in\_max}}$ after each optimization and repeating the optimization with the new parameters, but it is a less attractive option because of the time-consuming nature and uncertainty of manual iterations. The digital goal function provides a balance between efficiency and distortion minimization to achieve maximum power margin and is easy to use because it is a single quantity optimization.

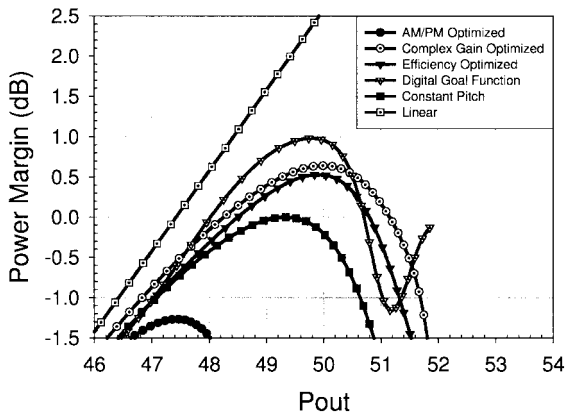


Fig. 7. Relative power-margin performance for the optimized helix TWT circuits.

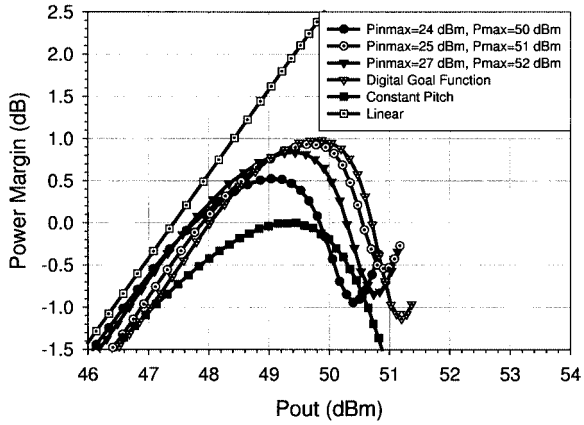


Fig. 8. Complex optimization after digital goal function optimization.

For relatively lower order modulations, the digital goal function essentially attempts to equalize the gain at a limited number of input drive levels. For 16 QAM, this number is only three. Therefore, a TWT circuit that is optimized for a maximum power margin at a particular drive level might sacrifice the power margin at other drive levels. This is demonstrated in Fig. 8. In Fig. 8, the helix profile optimized with the digital goal function in Fig. 6 is used as the initial pitch profile for re-optimization with the complex goal function for three different pairs of ($P_{\text{in\_max}}$, $P_{\max}$). Each of the re-optimizations lowers the maximum power margin, but shows improvement before the maximum. As higher order modulation is used, the digital goal function will equalize the gain at more input drive levels. Complex-gain re-optimization will not create much difference. This implies that, for higher order modulations, a digital goal function optimized circuit will also be complex gain optimized. A complex gain optimized circuit is, however, not necessarily digital goal function optimized. This is because of the need to choose ($P_{\text{in\_max}}$, $P_{\max}$) for complex gain optimization, which is more susceptible to being trapped in a local minimum depending on the particular optimization algorithm implemented in the optimizer.

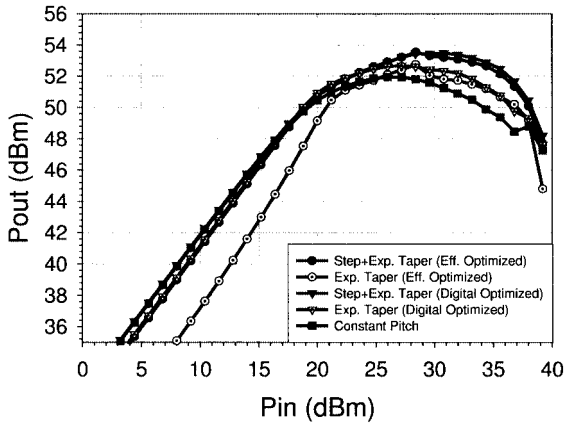


Fig. 9. Nonlinear amplitude conversion for constrained optimization.

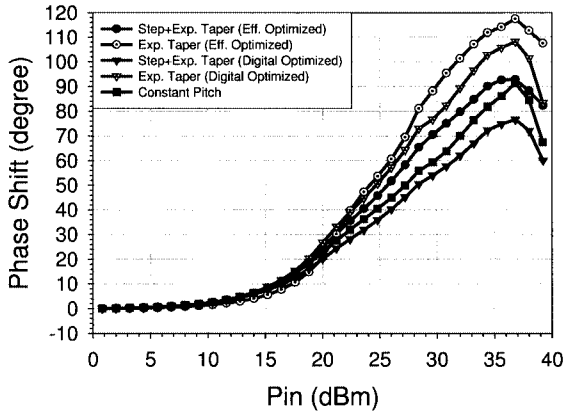


Fig. 10. Nonlinear phase conversion for constrained optimization.

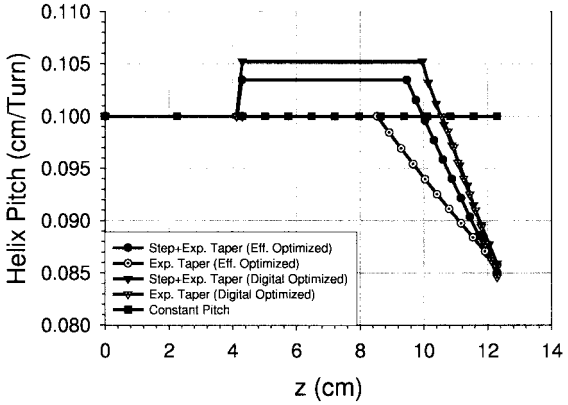


Fig. 11. Helix profiles for constrained optimization.

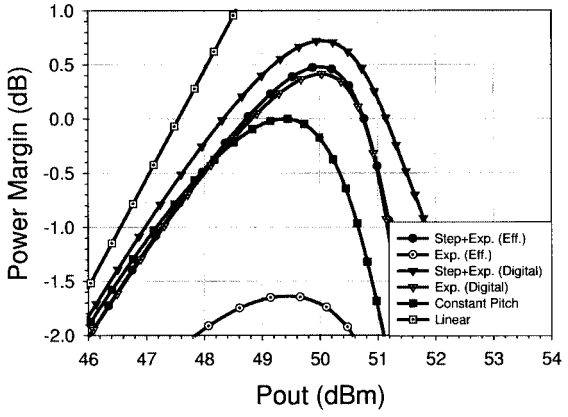


Fig. 12. Relative power-margin performance for constrained optimization.

### *B. Fixed-Shape Constrained Helix-Profile Optimization*

Due to the large degrees of freedom required for the approach described in Section IV-A, it is very difficult to control the shape of the helix profile. The shape of the optimized helix profiles tends to be irregular and have large variations. They are also very difficult to fabricate and it is likely that the improvement in the power margin could well be overwhelmed by additional issues such as internal reflection, etc. A better approach would be to require the pitch profile to have some fixed shape with parameters relating to the shape of those curves as the optimization parameters.

It was pointed out by Kosmahl [8] that the preferred rate of helix taper in a DVT configuration is an exponential rate with the taper starting at a location when the electronic efficiency is low. This suggests, for optimization, an exponential taper

$$\lambda_H(z) = \lambda_o \left[1 + \alpha \left(e^{b(z-z_0)} - 1\right)\right] \tag{9}$$

where $\lambda_H(z)$ is the pitch profile for the tapered section, $\lambda_0$ is the untapered pitch, $z_0$ is the starting location of the taper section, and $\alpha$ and $b$ are constants to be determined.

Optimization runs were carried out with the constraint that $\lambda_H(z)$ satisfies (9). Two sets of optimization parameters were used: 1) $\alpha$, $b$, and $z_0$ are the optimization parameters with $\lambda_0$ fixed and equal to the helix pitch before the sever; 2) $\alpha$, $b$, and $z_0$, as well as $\lambda_0$ are the optimization parameters with the helix pitch before the sever fixed. The configuration in (1) is the original DVT configuration described in [8]. Also, we only used efficiency and digital goal functions. The characteristics for four of the optimized circuits are shown in Figs. 9–12. The drive curves are shown in Figs. 9 and 10, the helix-pitch profile is shown in 11, and the power margin is shown in 12. The power-margin curves are calculated by estimating the BER using the drive curves in Figs. 9 and 10 with a BER of $10^{-5}$. Note that, in each of the optimized helix-pitch profiles in Fig. 11, the optimized value for the $b$-parameter for each of the optimized helix profiles is very close to zero and the exponentially tapered section can essentially be replaced by a linear taper without changing the TWT performance.

For the same set of optimization parameters, the efficiency and digital goal functions result in approximately the same maximum output power with the efficiency optimization having slightly higher maximum output power. The digital goal function, on the other hand, always produces drive curves with less AM/PM distortion that always translates into a higher power margin.

Allowing $\lambda_0$ to vary during optimization produces a phase velocity step after the sever. This step and the phase velocity taper at the end of the helix result in drive curves with higher maximum output and lower AM/PM distortion and, therefore, also higher power margin. The lower AM/PM distortion is understandable if we recall that the helix pitch for the AM/PM optimization in Section IV-A is greater than the constant pitch value in the entire helix after the sever.

Even though the maximum power-margin improvement from the constant pitch TWT is approximately 0.7 dB, which is less than the 1-dB improvement achieved in Section IV-A, the pitch profiles in Section IV-B are much easier to realize that those in Section IV-A. It is also reasonable to suggest that even higher power-margin improvement can be achieved by optimizing other helix-pitch profiles that are more efficient in suppressing nonlinearity in a TWT. We also note that helix pitch is not the only circuit parameter that can be optimized to improve power margin. Other circuit parameters such as the helix radius and sever width can be used together with the pitch profile to achieve this goal, as described in the many inventions listed in [10]–[13].

## V. Conclusion

In this paper, a procedure for the optimization of TWT operation and physical design based on the power margin has been examined. Although the established traditional figures-of-merit such as efficiency and complex gain can lead to TWTA designs performing better than unoptimized untapered helix designs, the use of a system-specific power margin as a figure-of-merit has been shown to lead to further improvement in TWTA designs. The improved TWTA design can yield beneficial improvement in the link margin for communication systems using spectrally efficient modulations.

The use of a power margin provides a figure-of-merit that balances both efficiency and linearity, and a quantitative analysis for a particular TWT circuit configuration; the use of iterative optimization provides a tool to fully explore its potential.

## Appendix

### *Approximation of Power Margin*

Our objective for the approximation is to derive a mathematical expression that has the general trend of the exact power-margin curve and enough free embedded parameters that can be adjusted to improve the accuracy by fitting the expression to the exact calculation, while minimizing computation time.

For a square 16-QAM constellation

$$\text{Error\_Rate} \approx \frac{1}{4}\sum_{i=1}^{12}\frac{1}{2}erfc\left(\frac{d_i}{\sigma}\right) \tag{A.1}$$

where $erfc(\,)$ is the complementary error function, $d_i$ is the distance from a recovered symbol to one of its decision boundary in the first quadrant of the I/Q plane, as shown in Fig. 3, and $\sigma$ is the rms noise level.

In the linear case, the recovered symbol locations coincide with the reference symbol locations, thus, we have

$$\text{Error\_Rate} \approx \frac{12}{8}erfc\left(\frac{d_0}{\sigma}\right) \tag{A.2}$$

where $d_0$ is the distance from a symbol to its decision boundary.

In the nonlinear case, the recovered symbol locations will no longer coincide with the reference symbol locations. Due to the fast drop rate of $erfc(\,)$, the error rate is dominated by a number of smallest distances. If we keep $m$ smallest distances ($m$ to be determined later),

$$\text{Error\_Rate} \approx \frac{1}{8}\sum_{i=1}^{m}erfc\left(\frac{d_i^s}{\sigma}\right) \tag{A.3}$$

where $d_1^s \le d_2^s \le d_3^s \cdots \le d_m^s$.

In order to maintain the same error rate in the presence of nonlinear distortion, we need to have

$$\frac{12}{8}erfc\left(\frac{d_0}{\sigma}\right) = \frac{1}{8}\sum_{i=1}^{m}erfc\left(\frac{d_i^s}{\sigma}\right). \tag{A.4}$$

For low error rate, $(d/\sigma) \gg 1$, and we have the following loose approximation for $erfc(\,)$:

$$erfc\left(\frac{d}{\sigma}\right) \sim \left(\frac{\sigma}{d}\right)^{2n} \tag{A.5}$$

where $n$ depends on the required error rate. Combining (A.4) and (A.5), we have

$$12\left(\frac{\sigma}{d_0}\right)^{2n} = \sum_{i=1}^{m}\left(\frac{\sigma}{d_i^s}\right)^{2n} \tag{A.6}$$

and

$$\left(\frac{\left(\frac{D}{\sigma}\right)^2}{\left(\frac{d_0}{\sigma}\right)^2}\right)^n = \frac{1}{12}\sum_{i=1}^{m}\left(\frac{D}{d_i^s}\right)^{2n} \tag{A.7}$$

where $D$ is the distance from one of the reference constellation to its decision boundary. Power penalty (in decibels) is, therefore, given by

$$\begin{aligned}\text{Penalty(dB)} &= 10\log_{10}\left(\frac{\left(\frac{D}{\sigma}\right)^2}{\left(\frac{d_0}{\sigma}\right)^2}\right)\\ &= 10\frac{1}{n}\log_{10}\left(\frac{1}{12}\sum_{i=1}^{m}\left(\frac{D}{d_i^s}\right)^{2n}\right)\end{aligned} \tag{A.8}$$

and the power margin is given by

$$\begin{aligned}\text{Power\_margin(dB)} = \overline{P_{\text{out}}}\text{(dB)} &- 10\frac{1}{n}\log_{10}\\ &\times\left(\sum_{i=1}^{m}\left(\frac{D}{d_i^s}\right)^{2n}\right) + a\end{aligned} \tag{A.9}$$

where $a$ is a constant and, if only the relative power margin is of interest, its exact value is not important and can be ignored.

A similar expression can be derived for higher order M-QAM. The $m$- and $n$-parameters in (A.9) can be determined by fitting (A.9) to exactly calculated power-margin curves for M-QAM modulation, as shown in Fig. 13, and are summarized in Table I. The parameter $a$ depends on the modulation, as well as the parameters $m$ and $n$. It should be held fixed when comparing the relative power margin for different drive curves with the same modulation format. In Fig. 14, the relative power margin for 16-QAM modulation for four optimized drive curve used in Section IV, as well as their approximation is plotted. The agreement

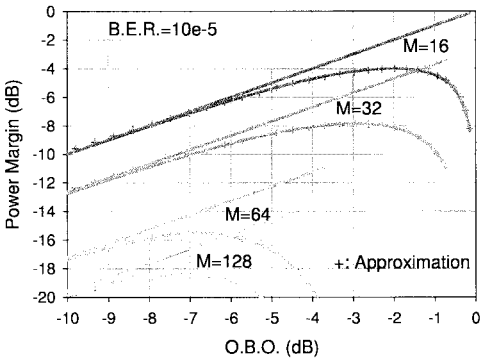


Fig. 13. Comparison of the calculated power margin with digital goal function approximation for M-QAM modulation. The symbols are an approximation and the solid lines are an exact calculation.

TABLE I
PARAMETERS $m$ AND $n$ SUMMARY

| m-QAM | M=16 | M=32 | M=64 | M=128 |
|---|---|---|---|---|
| $m$ | 4 | 8 | 16 | 32 |
| $n$ | 6.5 | 6.5 | 6.0 | 6.0 |

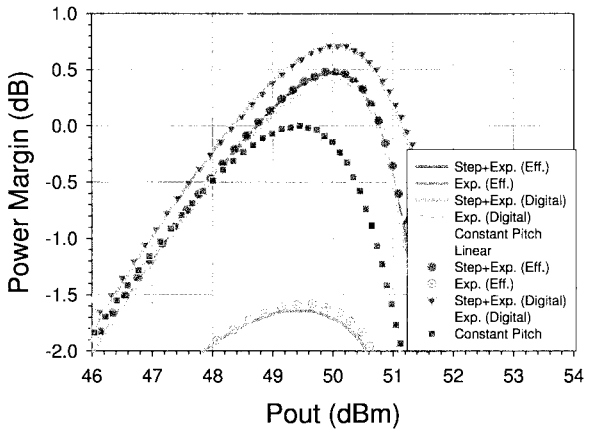


Fig. 14. Comparison of the calculated relative power margin with digital goal function approximation for different nonlinear drive curves. The symbols are the approximation and the solid lines are the exact calculation.

between the exact calculation and the approximation is excellent.

## ACKNOWLEDGMENT

The authors would like to thank Dr. J. P. Calame, Naval Research Laboratory (NRL), Washington, DC, and Dr. P. Safier, Science Applications International Corporation, McLean, VA, for useful discussions. The authors greatly appreciated the loan of the 8573H TWTA by Boeing Electron Dynamic Devices for experimental tests.

## REFERENCES

[1] A. Katz, "Linearization: Reducing distortion in power amplifiers," *IEEE Microwave Mag.*, vol. 2, pp. 37–49, Dec. 2001.

[2] C. J. Clark, G. Chrisikos, S. Muha, A. A. Moulthrop, and C. P. Silva, "Time-domain envelope measurement technique with application to wide-band power amplifier modeling," *IEEE Trans. Microwave Theory Tech.*, vol. 46, pp. 2531–2540, Dec. 1998.

[3] M. C. Jeruchim, P. Balaban, and K. S. Shanmugan, *Simulation of Communication Systems*. New York: Plenum, 1992.

[4] A. A. M. Saleh, "Frequency-independent and frequency-dependent nonlinear models of TWT amplifier," *IEEE Trans. Commun.*, vol. COM-29, pp. 1715–1720, Nov. 1981.

[5] J. Sombrin, "A new criterion for the comparison of TWT and linearized TWT and for the optimization of linearizers used in transmission systems," presented at the ESA/NATO TWTA Workshop, Apr. 1997.

[6] S. Pupolin and L. J. Greenstein, "Performance analysis of digital radio links with nonlinear transmit amplifiers," *IEEE J. Select. Areas Commun.*, vol. SAC-5, pp. 534–546, Apr. 1987.

[7] G. Karam and H. Sari, "Analysis of predistortion, equalization, and ISI cancellation techniques in digital radio system with nonlinear transmit amplifiers," *IEEE Trans. Commun.*, vol. 37, pp. 1245–1753, Dec. 1989.

[8] H. G. Kosmahl, "Linearized traveling wave amplifier with hard limiter characteristics," U.S. Patent 4 564 787, Jan. 14, 1986.

[9] A. S. Gilmour, Jr., *Principles of Traveling Wave Tubes*. Boston, MA: Artech House, 1994.

[10] N. J. Dionne, "Traveling wave electron interaction device having efficiency enhancement means," U.S. Patent 3 614 517, Oct. 19, 1971.

[11] J. Wong, "Traveling wave tube linearity characteristics," U.S. Patent 3 758 811, Aug. 2, 1972.

[12] Y. Yuasa, Y. Morizumi, and R. Orui, "Traveling-wave tube having phase velocity tapering means in slow-wave circuit," U.S. Patent 4 107 572, Aug. 15, 1978.

[13] H. G. Kosmahl, "Tapered traveling wave tube," U.S. Patent 6 356 022 B1, Mar. 12, 2002.

[14] T. M. Antonsen, Jr. and B. Levush, "CHRISTINE: A Multifrequency parametric simulation code for traveling-wave tube amplifiers," NRL, Washington, DC, NRL Rep. 97-9845, 1997.

[15] ——, "Traveling-wave tubes with nonlinear dielectric elements," *IEEE Trans. Plasma Sci.*, vol. 26, pp. 774–786, June 1998.

[16] R. De Gaudenzi and M. Luise, "Analysis and design of an all-digital demodulator for trellis coded 16-QAM transmission over a nonlinear satellite channel," *IEEE Trans. Commun.*, vol. 43, pp. 659–668, Feb.–Apr. 1995.

[17] D. K. Abe, B. Levush, T. M. Antonsen, Jr., D. R. Whaley, and B. G. Danly, "Design of a linear $C$-band helix TWT for digital communications experiments using the CHRISTINE suite of large-signal codes," *IEEE Trans. Plasma Sci.*, vol. 30, pp. 1053–1062, June 2002.

[18] J. G. Proakis, *Digital Communications*. New York: McGraw-Hill, 2000.

[19] J. W. Craig, "A new, simple and exact result for calculating the probability of error for two-dimensional signal constellations," in *IEEE Military Communications Conf.*, 1991, pp. 571–575.

**Joe X. Qiu** (M'03) received the B.S. and Ph.D. degrees in physics from the State University of New York at Stony Brook, in 1991 and 1997, respectively.

From 1992 to 1997, he was a Graduate Research Assistant with the Accelerator Test Facility, Brookhaven National Laboratory, where he participated in a wide range of experimental studies related to high brightness electron beams and free-electron lasers. From 1997 to 2000, he was a National Research Council Post-Doctoral Research Associate with the Beam Physics Branch, Plasma Physics Division, Naval Research Laboratory (NRL), Washington, DC. Since 2000, he has been a Research Physicist with the Vacuum Electronics Branch, Electronics Science and Technology Division, NRL. His current research activities are concentrated on the studies of nonlinear distortions in vacuum electronics microwave PAs, in particular, TWTAs, their effects in high-date-rate communications, and the construction of new ultra-broad-band test and measurement systems for characterizing the distortions.

**David K. Abe** (S'89–M'92) received the B.S. degree in electrical engineering (with honors) from Harvey Mudd College, Claremont, CA, in 1981, the M.S.E.E. degree from the University of California at Davis, in 1988, and the Ph.D. degree in electrophysics from the University of Maryland at College Park, in 1992. His doctoral research concerned experimental studies of high-power overmoded backward-wave oscillators.

From 1982 to 1988, he was a Member of the Technical Staff with the Lawrence Livermore National Laboratory, Livermore, CA, where he supported the Nuclear Design Program. In 1992, he joined Berkeley Research Associates, Springfield, VA, where, until 1994, he was involved with pulsed- and high-power microwave projects. In 1994, he joined the Army Research Laboratory, Adelphi, MD, where he pursued projects in electromagnetic effects and high-power microwave generation. In 1997, he joined the Vacuum Electronics Branch, Naval Research Laboratory (NRL), Washington, DC, where he is currently pursuing research projects in the areas of linear beam slow-wave microwave devices and the electronic properties of materials.

Dr. Abe is a member of the American Physical Society.

**Thomas M. Antonsen, Jr.** (SM'87) was born in Hackensack, NJ, in 1950. He received the Bachelor's degree in electrical engineering, and Master's and Ph.D. degrees from Cornell University, Ithaca, NY, in 1973, 1976, and 1977, respectively.

From 1976 to 1977, he was a National Research Council Post-Doctoral Fellow with the Naval Research Laboratory (NRL), Washington, DC. From 1977 to 1980, he was a Research Scientist with the Research Laboratory of Electronics, Massachusetts Institute of Technology (MIT), Cambridge. In 1980, he joined the University of Maryland at College Park. In 1984, he was a faculty member with the Departments of Electrical Engineering and Physics. He is currently a Professor of physics and electrical and computer engineering with the University of Maryland at College Park. He has held visiting appointments with the Institute for Theoretical Physics (UCSB), the Ecole Polytechnique Federale de Lausanne, Switzerland, and the Institute de Physique Theorique, Ecole Polytechnique, Palaiseau, France. He has authored and coauthored over 200 journal papers and coauthored *Principles of Free-Electron Lasers* (London, U.K.: Chapman & Hall, 1992). His interests include the theory of magnetically confined plasmas, theory and design of high-power sources of coherent radiation, nonlinear dynamics in fluids, and the theory of the interaction of intense laser pulses and plasmas. He has served on the Editorial Boards of *Physical Review Letters*, *The Physics of Fluids*, and *Comments on Plasma Physics*.

Prof. Antonsen was selected as a Fellow of the Division of Plasma Physics, American Physical Society in 1986. In 1999, he was a corecipient of the Robert L. Woods Award for Excellence in Vacuum Electronics Technology. In 2003, he was the recipient of the IEEE Plasma Science and Applications Award.

**Bruce G. Danly** (M'87–SM'01–F'03) received the B.A. degree in physics from Haverford College, Haverford, PA, in 1978, and the Ph.D. degree in physics from the Massachusetts Institute of Technology (MIT), Cambridge, in 1983. His doctoral dissertation concerned the area of quantum electronics and high power infrared Raman lasers.

From 1983 to 1995, he was a member of the research staff with the MIT Plasma Fusion Center, initially as Research Scientist (1983–1992) and then as Principal Scientist (1992–1995). While with MIT, he participated in research on gyrotrons, free-electron lasers, relativistic klystrons, and other high-power RF source technologies for use in plasma heating and high-gradient RF linear accelerators. In 1995, he joined the Naval Research Laboratory (NRL), Washington, DC, as Head of the High Power Devices Section, Vacuum Electronics Branch. The High Power Devices Section carries out experimental research and development on new concepts for high-power microwave, millimeter-wave, and infrared sources based on both slow- and fast-wave interaction mechanisms. Technologies under investigation include the class of gyrotron amplifiers (gyroklystrons, gyrotwystrons, gyro-TWTs), free-electron lasers, TWTs, and klystrons.

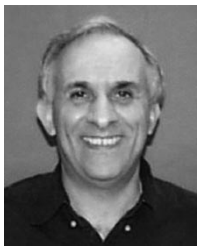

**Baruch Levush** (M'88–SM'90–F'01) received the M.Sc. degree in physics from the Latvian University, Riga, Latvia, and the Ph.D. degree in physics from Tel-Aviv University, Tel-Aviv, Israel.

In 1985, he joined the Institute for Plasma Research, University of Maryland at College Park, where his research focused on the physics of coherent radiation sources and the design of high-power microwave sources such as gyrotrons, TWTs, backward-wave oscillators, and free electron lasers. In 1995, he joined Naval Research Laboratory (NRL), Washington, DC, as the Head of the Theory and Design Section, Vacuum Electronics Branch, Electronics and Technology Division. He is actively involved in developing theoretical models and computational tools for analyzing the operation of vacuum electron devices and in inventing new concepts for high-power high-frequency coherent radiation sources. He is also responsible for developing a suite of new design codes for vacuum electron devices under the auspices of the Office of Naval Research Modeling and Simulation Project. He has coauthored over 130 journal papers.

Dr. Levush was the recipient of the 1999 Department of Defense (DoD) Robert L. Woods Award for his role in the successful development of a 10-kW average power $W$-band gyro-klystron.